Bull. Mater. Sci., Vol. 35, No. 5, October 2012, pp. 759–766. © Indian Academy of Sciences.

Synthesis and characterization of NiPcTSTNa(L) thin films

M E SÁNCHEZ-VERGARA[a,*], V GARCÍA-MONTALVO[b], J SANTOYO-SALAZAR[c], R J FRAGOSO-SORIANO[c] and O JIMÉNEZ-SANDOVAL[d]

[a]Facultad de Ingeniería, Universidad Anáhuac México Norte, Avenida Universidad Anáhuac 46, Col. Lomas Anáhuac, Huixquilucan, Estado de México 52786, México

[b]Instituto de Química, Universidad Nacional Autónoma de México, Circuito Exterior S/N, Ciudad Universitaria, México, D. F. 04510, México

[c]Centro de Investigación y de Estudios Avanzados del Instituto Politécnico Nacional, Unidad Zacatenco, Instituto Politécnico Nacional 2508, México, D. F. 07360, México

[d]Centro de Investigación y de Estudios Avanzados del Instituto Politécnico Nacional, Unidad Querétaro, Apartado Postal 1-798, Querétaro, Qro. 76001, México

MS received 8 September 2011

Abstract. **NiPcTSTNa(L) [L = ethylenediamine (EDA); 1,4-diaminobutane (BDA); and 2,6-diamineanthraquinone (AqDA)] thin films were deposited by thermal evaporation. Their surface morphology was studied by AFM and SEM, and their chemical composition determined by EDS. Optical absorption studies of NiPcTSTNa(L) films were performed in the 200–1150 nm wavelength range. The optical bandgap of thin films was determined from the $(\alpha h\nu)^{1/2}$ vs $h\nu$ plots for indirect allowed transitions. The temperature dependence of electrical conductivity shows a semiconducting behaviour. The amorphous semiconductor films show thermal activation energies of electrical conduction between 3·3 and 3·7 eV.**

Keywords. **Thin films; semiconductors; optical absorption; electrical conductivity.**

1. Introduction

Organic semiconducting materials are rapidly making an impact in the area of electronics and optoelectronics (Shafai and Anthopoulos 2001). Metallophthalocyanines (MPcs) are a prominent class of materials with electrical, optical and optoelectronic applications in many fields (de la Torre *et al* 2004; Campidelli *et al* 2008; Wojdyla *et al* 2008). One of the major advantages of using MPcs is their chemical stability as well as the ability to readily modify the molecular structure allowing the molecular engineering of their physical properties accordingly (Shafai and Anthopoulos 2001). High thermal stability of MPcs permits the deposition of high purity thin films through high-vacuum vapourization techniques (El-Nahass *et al* 2005a). Typically, the films exist as either α- or β-phases, or result in amorphous state depending mainly on the molecular self-stacking ability of the derivative, and also on the thin film fabrication procedure. The control of structure is of great importance in thin film technology since the main opto-electronic properties, such as the photogeneration of charge carriers, highly depend on the degree of molecular organization (Del Caño *et al* 2005). Because of the very good optical absorption of these molecules in the UV-vis region, there is considerable interest in the characterization of the electronic structures of phthalocyanines (El-Nahass *et al* 2005b). For thin films of H_2Pc, MgPc, FePc, CoPc, CuPc and ZnPc, the visible and near ultraviolet absorption spectra have been measured (Davidson 1992). Schmeisser *et al* (1991) found that the lowest absorption band at 1·73 eV is due to transitions between HOMO π and LUMO π^* molecular orbitals which, due to the size of the 18-π electron systems, are well separated in energy from the molecular orbital structure of the phenyl and aza groups. They recorded a considerably smaller energy gap for PbPc than for H_2Pc from the onset of the absorption spectrum, 1·2 eV. Bialek *et al* (2002) calculated the HOMO–LUMO gap of NiPc as 2·41 eV and suggested that the orbitals next to the HOMO are separated from each other by 1·84, 2·44, 0·17, 0·28 and 0·09 eV, respectively and the energy level of the second unoccupied molecular orbital is widely separated from the LUMO, with differences becoming smaller for the following orbitals. Although NiPc has been the subject of various investigations, considerably less attention has been paid on its structural and optical characterization (El-Nahass *et al* 2005a). In this communication, we report the determination of optical parameters related to the main transitions in the UV-vis region, as well as the corresponding optical bandgap calculations for non-crystalline thin films based on nickel(II) phthalocyanine–tetrasulfonic acid tetrasodium salt (NiPcTSTNa) and axial diamine ligands: ethylenediamine (EDA), 1,4-diaminobutane (BDA) and 2,6-diamineanthraquinone (AqDA). The films were prepared by thermal evaporation and characterized by FT–IR spectroscopy, AFM, SEM, EDS and ellipsometry

*Author for correspondence (elena.sanchez@anahuac.mx)

measurements. The refractive indices and absorption coefficients, parameters of particular interest for the design and fabrication of optoelectronic devices, have been determined for the films as well. Finally, temperature dependence of electrical conductivity has been investigated.

2. Experimental

The raw materials for this work were obtained from commercial sources and used without further purification. The characterization of the powder materials was carried out by FT–IR spectroscopy, in a Bruker spectrophotometer, model Tensor 27, as KBr pills in the 4000 to 300 cm^{-1} region. For the preparation of the films, a vacuum chamber was used with a diffusion pump and a special molybdenum crucible with a double-grid cover. A quartz fibre was put inside the crucible to avoid the ejection of grains towards the substrate at a temperature of 563 K. The material was deposited on Corning 7059 glass substrates, which were ultrasonically degreased in warm methanol and dried in nitrogen, and on single-crystalline *c*-Si wafers, which were chemically etched with a *p* solution (10 ml HF, 15 ml HNO_3 and 300 ml H_2O) in order to remove the native oxide from the substrate surface. The base pressure used in the evaporation process was 10^{-5} torr at room temperature. The crucible-substrate distance was 20 cm. For the SEM characterization of the films, a Jeol JSM 5200 CX microscope was used, at a 5 kV potential for all samples. Topography and roughness of surfaces were analysed by atomic force microscopy (AFM), model Autoprobe CP Thermomicroscopes in Tapping mode. The thickness measurements were made with a Sloan Dektak IIA profilometer. The FT–IR characterization was carried out using a Nicolet 205 spectrophotometer, on Si substrate deposited

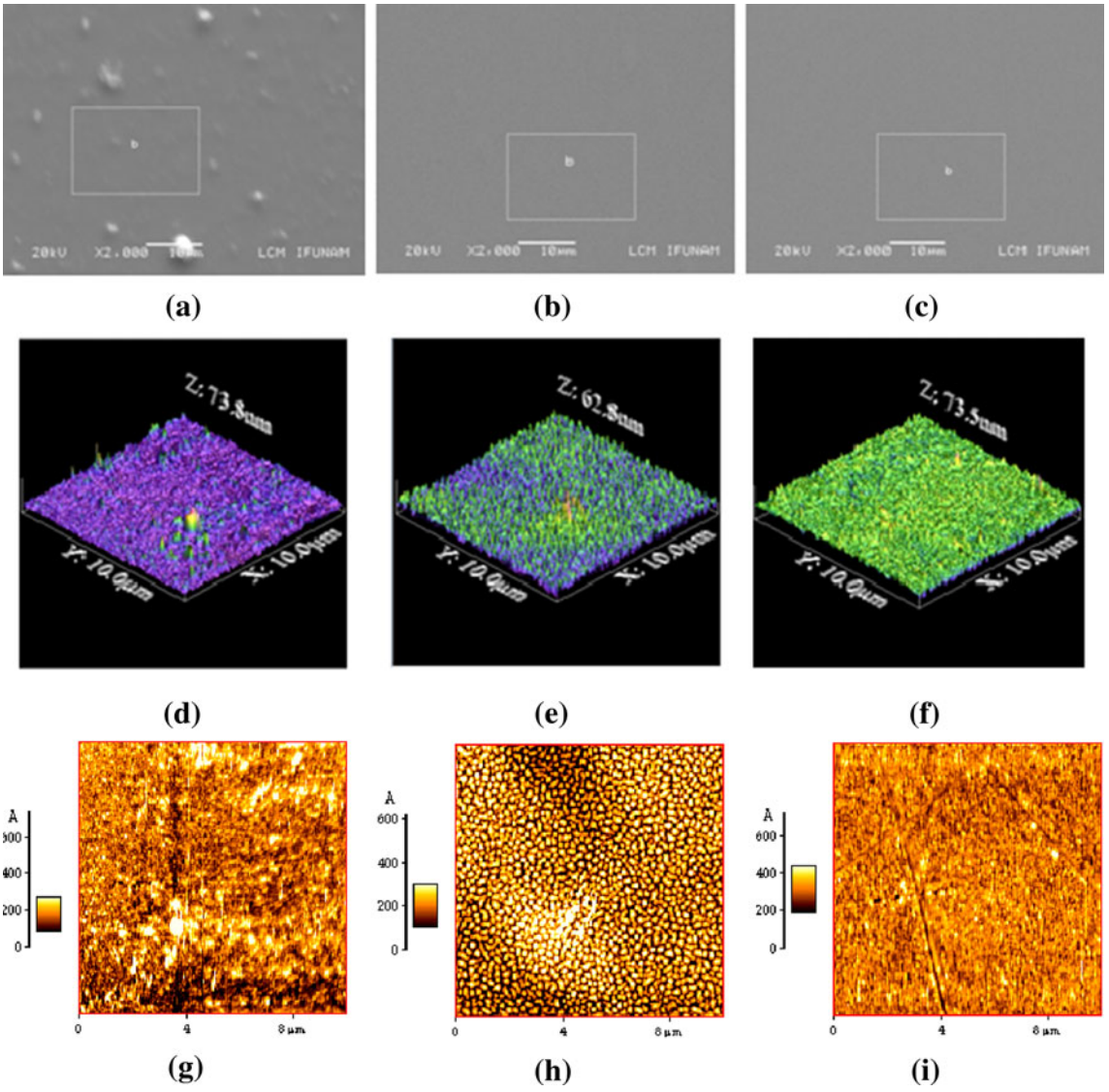

Figure 1. Morphology of NiPcTSTNa(EDA), NiPcTSTNa(BDA) and NiPcTSTNa(AqDA) films: (**a–c**) top view of SEM images; AFM (**d–f**) tapping-mode topographical and (**g–i**) phase images.

films, in the 4000 to 300 cm^{-1} range. The UV-visible studies were performed in a Unicam spectrophotometer, model UV300, on glass substrate deposited films. Ellipsometry was carried out in a Gaertner Scientific Corporation ellipsometer (model L117), with a He–Ne laser (630 nm), using films deposited on silicon wafers. A four-probe press contact method was used to measure electrical conductivity of the sample within a working-temperature range between 360 and 473 K. The temperature dependence of the electrical conductivity of the sample in this range was measured with a Keithley 230 programmable voltage source and a Keithley 485 auto-ranging pico-ammeter, both PC-controlled.

General procedure: A solution of the NiPcTSTNa salt ($C_{32}H_{12}N_8Na_4NiO_{12}S_4$) in absolute ethanol was added to a solution of the appropriate diamine ligand [ethylenediamine (EDA), 1,4-diaminebutane (BDA) or 2,6-diamineanthraquinone (AqDA)] in the same solvent. The resultant mixture was maintained under reflux for about 3 days until a precipitate was obtained. The product was then filtered, washed with distilled water and absolute ethanol to eliminate unreacted diamine and phthalocyanine, respectively and then dried in vacuum.

NiPcTSTNa(EDA): 0·40 g (0·41 mmol) of $C_{32}H_{12}N_8Na_4NiO_{12}S_4$ in 20 mL ethanol, 10 mL of ethylenedyamine (excess) in 10 mL ethanol. Violet powder, yield 82%, m.p. 335 °C (dec).

NiPcTSTNa(BDA): 0·21 g (0·21 mmol) of $C_{32}H_{12}N_8Na_4NiO_{12}S_4$ in 15 mL ethanol, 0·42 g (4·8 mmol) of 1,4-diaminebutane in 15 mL ethanol. Magenta powder, yield 86%, m.p. 340 °C (dec).

NiPcTSTNa(AqDA): 0·20 g (0·20 mmol) of $C_{32}H_{12}N_8Na_4NiO_{12}S_4$ in 15 ml of ethanol, 0·40 g (1·6 mmol) of 2,6-diamineanthraquinone in 15 mL ethanol. Violet powder, yield 72%, m.p. 340 °C (dec).

3. Results and discussion

Surfaces of NiPcTSTNa(EDA), NiPcTSTNa(BDA) and NiPcTSTNa(AqDA) samples were scanned by AFM and SEM. Topography obtained by AFM showed roughness, RMS, with a wrinkle height of 66·4 nm for NiPcTSTNa(EDA); 39 nm for NiPcTSTNa(BDA) and 49·9 nm for NiPcTSTNa(AqDA). The difference in roughness between these three samples could be correlated with type of amine in each molecular material (Ottaviano *et al* 1997). These non-crystalline thin films showed homogeneity in a continuum media, which were steady along surface for each sample. These features were substantiated by typical top-view SEM images (figures 1a–c) and compound analysis, EDS. 3D topography and phase images at 10×10 μm (figures 1d–f and 1g–i) reveal thin films spreading where the presence of granular aggregates is observed.

An EDS analysis was performed to determine the chemical composition of the novel molecular materials. Figure 2 shows EDS spectrum for NiPcTSTNa(AqDA), where presence of the reference elements for both donor and acceptor species is observed. Analogous results were obtained for other compounds.

A comparison of IR absorption spectra of powder and thin film forms deposited on fresh cleavage KBr single crystal indicated that the thermal evaporation technique is a good technique to obtain NiPc stoichiometric thin films (El-Nahass *et al* 2005b). IR spectra of the powder samples show characteristic absorption bands at 1560, 1140, 1068,

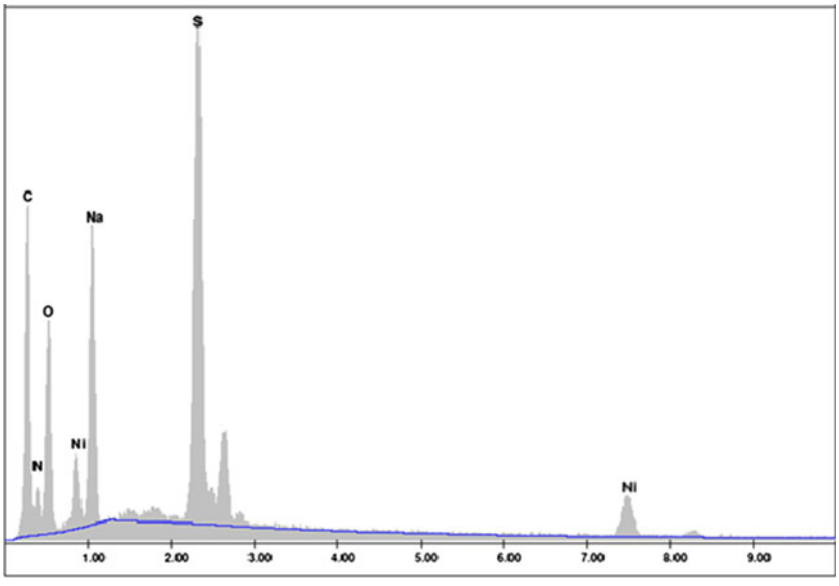

Figure 2. EDS spectrum for NiPcTSTNa(AqDA).

970, 885 and 740 cm^{-1}, and around 1330 and 1060 cm^{-1} of the original metal phthalocyanine–tetrasulfonate. Also, N–H stretching bands around 3400 and 3335 cm^{-1} indicate the presence of NH_2 and NH groups. The band around 1728 cm^{-1} corresponds to N–H bending vibrations and that at 2940 cm^{-1} to C–H stretching vibrations of the aliphatic chain of the amine ligands in NiPcTSTNa(EDA) and NiPcTSTNa(BDA). Additionally, NiPcTSTNa(AqDA) exhibits a strong C=O stretching vibration band at 1628 cm^{-1}. The peaks in the 700–400 cm^{-1} interval originate most probably from vibrations in the benzene ring in interaction with the pyrrole ring. The main peak at 730 cm^{-1} is attributed to non-planar deformation of C–H bonds of benzene rings (El-Nahass *et al* 2005b). The medium band at 755 cm^{-1} and a band at 779 cm^{-1} also correspond to non-planar vibrations of the C–H bonds (El-Nahass *et al* 2005b).

The UV-visible spectra in the 200–1150 nm wavelength range for the NiPcTSTNa(L) films, obtained at room temperature, are shown in figure 3. The bands originate from molecular orbitals within the aromatic 18π electron system and from overlapping orbitals on the metal central atom (Ottaviano *et al* 1997; El-Nahass *et al* 2005a; Seoudi *et al* 2006). The band of the phthalocyanine molecule, viz Q band, appears in the region between 550 and 750 nm. The distinct characteristic peaks of NiPcTSTNa(L) in the visible region have been generally interpreted in terms of π–π^* excitations between bonding and antibonding molecular orbitals. The energy peak of the Q band has been explained in different ways: as a second π–π^* transition, as an excitation peak, as a vibrational internal interval and as a surface state (Ottaviano *et al* 1997; El-Nahass *et al* 2005a; Seoudi *et al* 2006). The Q-band is associated with the amine coordination with the metallic ion in phthalocyanine. The presence of this absorption band may be interpreted as an overlap of π orbitals through the bidentate ligand. The conjugated double bonds within the structure of the films create electron orbitals overlapping between the molecules (π orbitals). Electrons are, therefore, able to transfer energy throughout the structure and become responsible for the absorption spectra (Sánchez Vergara *et al* 2008).

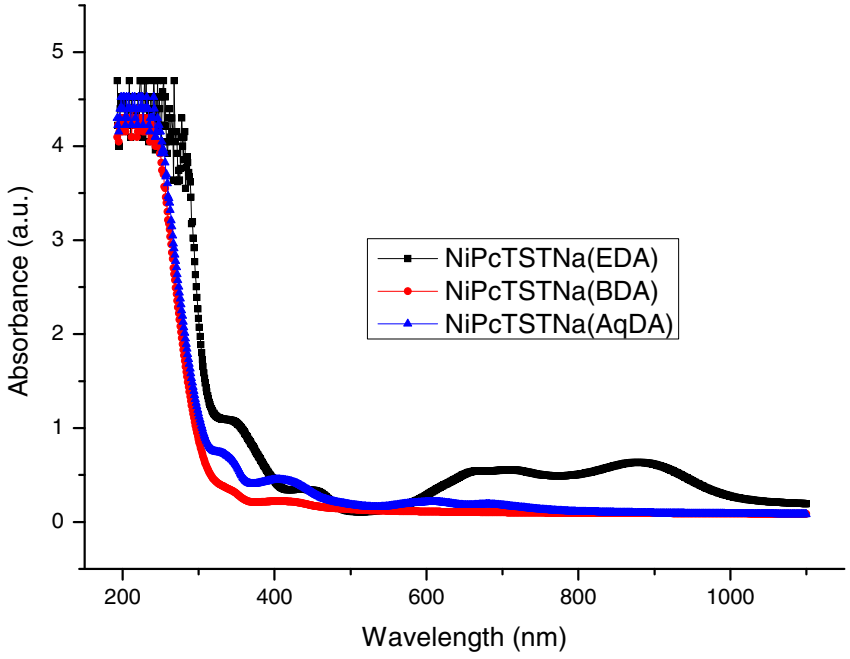

Figure 3. Electronic absorption spectra for NiPcTSTNa(EDA), NiPcTSTNa(BDA) and NiPcTSTNa(AqDA) thin films.

Table 1. Thickness, refractive index, optical activation energy and electrical parameters for NiPcTSTNa(EDA), NiPcTSTNa(BDA) and NiPcTSTNa(AqDA) thin films.

Thin film parameter	NiPcTSTNa(EDA)	NiPcTSTNa(BDA)	NiPcTSTNa(AqDA)
Film thickness (Å)	320	1684	1355
Refraction index	1·75	1·63	1·585
Optical activation energy (eV)	3·78	3·82	3·88
Electrical conductivity at 25°C (S/cm)	$2{\cdot}2 \times 10^{-3}$	$1{\cdot}5 \times 10^{-3}$	$4{\cdot}5 \times 10^{-2}$
Electrical activation energy (eV)	3·7	3·3	3·7

The refractive index, n (table 1), which was used to calculate the reflectance percentage from (1), was obtained from ellipsometry measurements.

$$R = \frac{100\,(n-1)^2}{(n+1)^2}. \tag{1}$$

The reflectance percentages of NiPcTSTNa(EDA), NiPcTSTNa(BDA) and NiPcTSTNa(AqDA) were 7%, 5·9% and 5%, respectively. On the basis of these results, use of Tauc's (1972) model to interpret the energy dependence of the absorption spectra of the deposited thin films seems valid. The two main conditions to apply this model are: (i) the semiconductor material must be amorphous and (ii) the values for the estimated reflectance must be below 15%.

The spectral distribution of the absorption coefficient, α, for the deposited NiPcTSTNa(L) thin films is shown in figure 4. As observed, the behaviour is similar to that of the absorption spectra. The optical absorption coefficient describes the depth of penetration of radiation into a bulk solid. The absorption coefficient is defined by the Beer–Lambert Law and can be calculated from the optical transmittance.

$$\alpha = -\ln T/t, \tag{2}$$

where T is the transmittance, related to the absorbance A by $A = -\log(T)$, t the film thickness. The thickness of the films ranged between 320 and 1684 Å (table 1).

The optical bandgap was determined from the analysis of the spectral dependence of the absorption near the fundamental absorption edges. In the above two regions the absorption coefficient, α, is well described by the Urbach's relation:

$$\alpha h\nu = \beta\left(h\nu - E_g\right)^n, \tag{3}$$

where $h\nu$ is the energy of incident photons and E_g the value of the optical bandgap corresponding to transitions indicated by a value of n. The factor, β, depends on the transition probability and can be assumed to be constant within the optical frequency range. Plots of $\alpha^{1/2}$ vs $h\nu$ near the absorption edge of the Q band for the deposited films produce a linear fit over a wider range in $h\nu$ as shown in figure 5. This is the characteristic behaviour of indirect transitions in amorphous semiconductors. In this kind of materials, the optical transitions are dominated, to a first approximation, by the so-called indirect transitions. In these electronic transitions from states in the valence band to states in the conduction band, there is no conservation of the electronic momentum (Cody 1984). This type of transitions is in agreement with Kumar *et al* (2000) for free and rare-earth complexed pthalocyanine and in disagreement with Collins *et al* (1993), Ambily and Menon (1999), and El-Nahass *et al* (2001) for PbPc, CuPc, and FePc thin films, respectively. The electron transport in the films reported in this work is strongly influenced by their molecular structures and the generation of Frenkel-type, tightly-bound excitons (Burns 1990). It has been noticed (Hill *et al* 2000) that significant charge localization in organic molecular materials leads to a significant difference between size of the optical gap and size of the transport gap, which corresponds to the energy of formation of a separated free electron and a hole. Whereas the optical

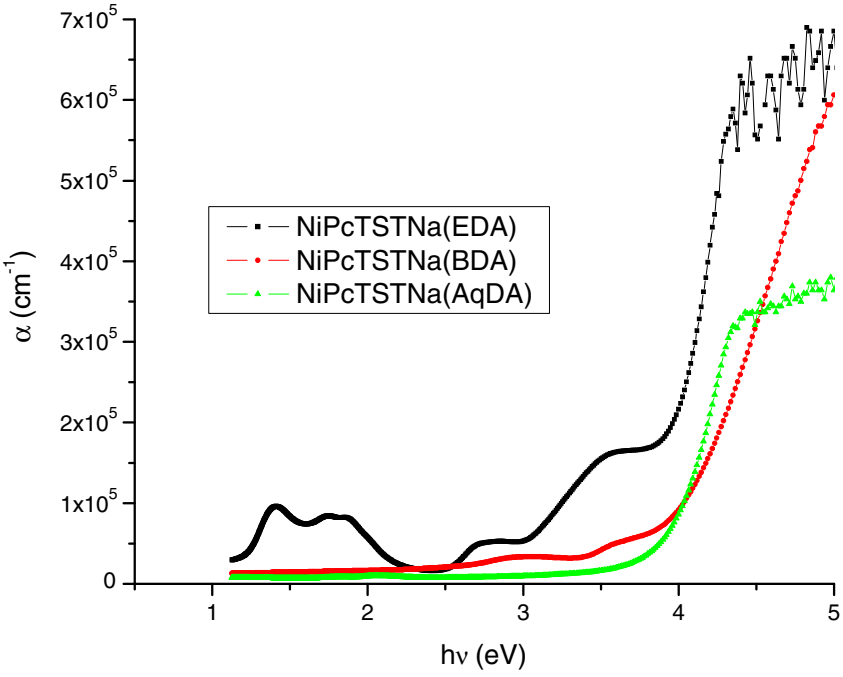

Figure 4. Plot of α vs $h\nu$ of NiPcTSTNa(EDA), NiPcTSTNa(BDA) and NiPcTSTNa(AqDA) thin films.

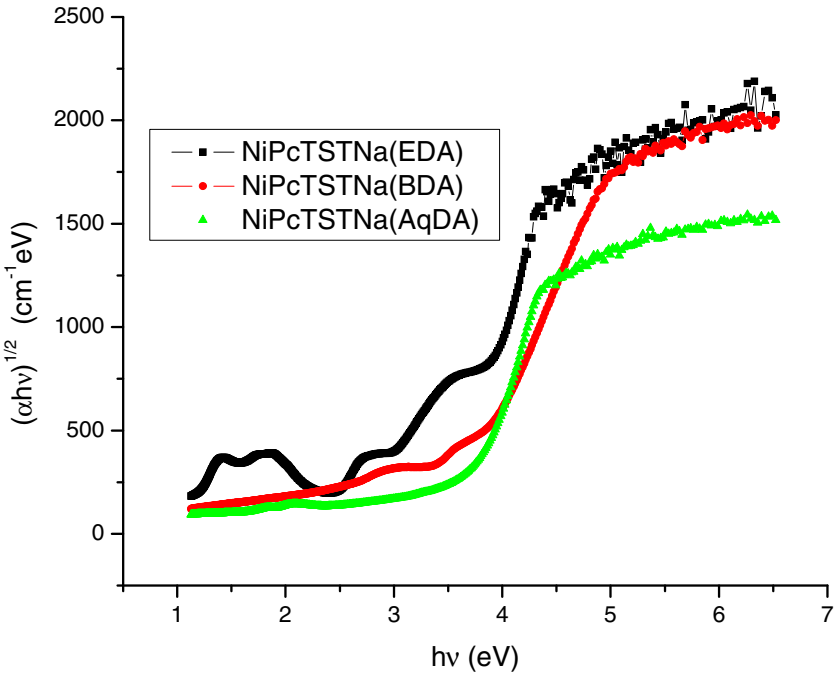

Figure 5. Plot of $(\alpha h\nu)^{1/2}$ vs $h\nu$ of NiPcTSTNa(EDA), NiPcTSTNa(BDA) and NiPcTSTNa(AqDA) thin films.

gap can be measured by optical absorption spectroscopy, the transport gap can be measured by ultraviolet or inverse photoemission spectroscopy and it is larger than the optical gap by a quantity equal to the binding energy of the Frenkel excitons. The energy gaps obtained are listed in table 1 and do not show important differences. This may be attributed to the fact that the charge transport in the materials is mainly related to the metal phthalocyanine, independently from the amine ligand. If it is considered that the optical activation energy values for semiconductors are located in the range between 1 and 3 eV, it can be inferred that the obtained thin films show a quite semiconductor-like behaviour, as their optical activation energies are around 3·8 eV.

The variation of electrical current with temperature was evaluated by using the four-probe method. This is one of the most used techniques for resistivity measurements in the semiconductor industry. Such tests are made on a line along the film, with equal spaces between the selected points; also, the current flow must be low enough to prevent sample heating, the voltmeter must have a high input impedance and measurements must be performed for several contact points, so that any injected minority charge carrier recombines. Temperature was measured by means of a chromel/alumel thermocouple mounted in close proximity to the specimen of interest. Electrical characterization was performed over a voltage range appropriate to the thickness of the sample (Abdel-Malik *et al* 1995; Shafai and Anthopoulos 2001). Figure 6 shows typical temperature dependence of the electrical conductivity of the films during heat treatment. By analysing the shape of the $\ln\ \sigma = f(10^3/T)$ plots, useful information regarding the processes occurring in the samples during treatment can be obtained; additionally, it provides support to the consideration that the model based on the bandgap representation could explain the electronic transfer mechanism in the films. Therefore, the estimate of some characteristic parameters of these materials has been made by using the expressions deduced for the intrinsic conduction domain of semiconductors. From figure 6, electrical conductivity of each material was evaluated at 25 °C. The results are shown in table 1. The NiPcTSTNa(AqDA) material shows highest conductivity at ambient temperature. It can also be observed that the electrical conductivity values for all the films are within the range for semiconductor materials (10^{-6} to $10^{1}\ \Omega^{-1}\ \mathrm{cm}^{-1}$) (Sánchez Vergara *et al* 2008). This is an important fact, since a molecular semiconductor is generally defined in terms of its room temperature conductivity and its behaviour with temperature.

It is known that the temperature dependence of electrical conductivity, σ, for a semiconductor material in its intrinsic conduction domain, is described by the following law (Sánchez Vergara *et al* 2008):

$$\sigma = \sigma_m \exp\left(-\frac{\Delta E_m}{KT}\right), \tag{4}$$

where σ_m is the pre-exponential factor and ΔE_m the activation energy for electrical conductivity. Calculated values of ΔE_m are presented in table 1. Such values are similar to those obtained for the optical bandgap. This fact suggests that ΔE_m is an activation energy involving both the energy necessary to excite electrons from the localized states toward extended states through the mobility edge and the electrical conduction by means of hopping mechanism between localized states.

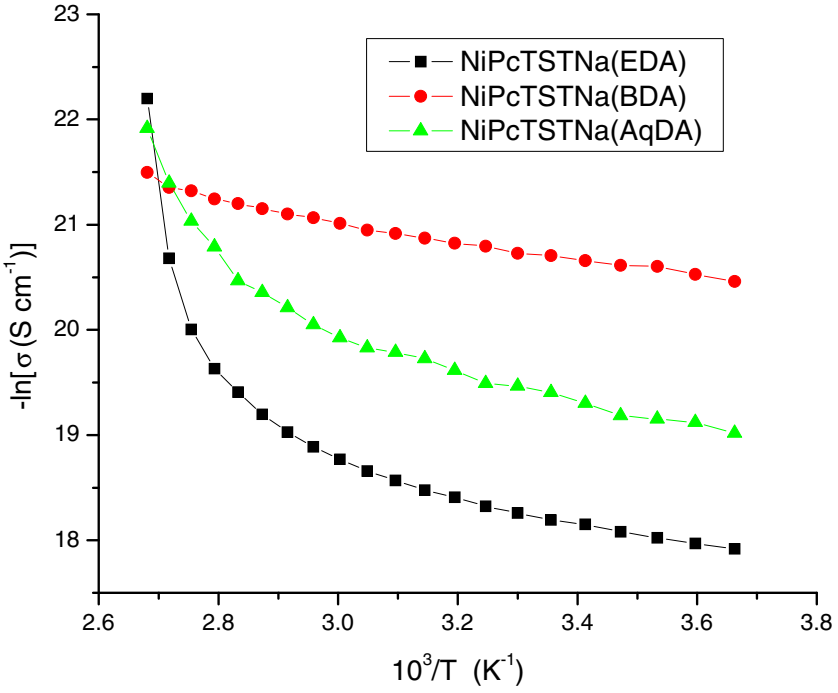

Figure 6. Temperature dependence of electrical conductivity of NiPcTSTNa(EDA), NiPcTSTNa(BDA) and NiPcTSTNa(AqDA) thin films.

Therefore, considering the optical and electrical properties of the deposited molecular films, their application in electronic and opto-electronic devices seems quite feasible.

4. Conclusions

Thin films of molecular materials of the NiPcTSTNa(L) type were deposited by vacuum thermal evaporation. According to their FT–IR spectra, they are formed by the same chemical units as those of the corresponding synthesized powders. Thus, the thermal evaporation process can be, in general, considered as a molecular process. The optical characterization of the deposited thin films was performed in the 200–1150 nm spectral range. The spectral distribution of the absorbance and the absorption coefficient of the NiPcTSTNa(L) films characterized by distinct peaks in the visible region has generally been interpreted in terms of π–π^* excitations. It is considered that π–d transitions are involved since NiPcTSTNa(L) has a partially occupied d-band. NiPcTSTNa(L) films show typical semiconducting characteristics. The electron transport in these materials is strongly influenced by the phthalocyanine. The model based on the bandgap representation was successfully used to explain the electron transfer mechanism in the compounds studied. The material, NiPcTSTNa(AqDA), has the highest conductivity, and in general, the electrical conductivity values at room temperature for all the compounds are within the range for semiconductor materials (10^{-6} to 10^{1} Ω^{-1} cm^{-1}). On the basis of the optical bandgap values, magnitude of the electrical conductivities and feasibility of preparing these compounds as thin films, it can be concluded that these materials may have a potential use in electronic device fabrication.

References

Abdel-Malik T G, Abdel-Latif R M, El-Samahy A E and Khalil S M 1995 *Thin Solid Films* **256** 139
Ambily S and Menon C S 1999 *Thin Solid Films* **347** 284
Bialek B, Kim I G and Lee J I 2002 *Synth. Met.* **129** 151
Burns G 1990 *Solid state physics* (San Diego: Academic Press, Inc.)
Campidelli S *et al* 2008 *J. Am. Chem. Soc.* **130** 11503
Cody G D 1984 *Hydrogenated amorphous silicon, Part B, Optical properties, semiconductors and semimetals*, J I Pankove (ed.), (Orlando: Academic Press) **Vol. 21**
Collins R A, Krie A and Abass A K 1993 *Thin Solid Films* **229** 113
Davidson A T 1992 *J. Chem. Phys.* **77** 168
de la Torre G, Vazquez P and Torres T 2004 *Chem. Rev.* **104** 3723
Del Caño T, Parra V, Rodríguez M L, Méndez R F, Aroca R F and De Saja J A 2005 *Appl. Surf. Sci.* **246** 327
El-Nahass M M, Soliman H S, Farid H S, Farag A A M and El-Shazly A A 2001 *J. Opt.* **30** 121
El-Nahass M M, Farag A M, Abd-El-Rahman K F and Darwish A A A 2005a *Opt. Laser Technol.* **37** 513
El-Nahass M M, Abd-El-Rahman K F and Darwish A A A 2005b *Mater. Chem. Phys.* **92** 185
Hill I G, Kahn A, Soos Z G and Pascal R A Jr 2000 *Chem. Phys. Lett.* **327** 181
Kumar G A, Thomas J, George N, Kumar B A, Shnan P R, Poori V P N, Vallabhan C P G and Unnikrishanan N V 2000 *Phys. Chem. Glasses* **41** 89

Ottaviano L, Di Nardo S, Lozzi L, Passacantando M, Picozzi P and Santucci S 1997 *Surf. Sci*. **373** 318

Sánchez Vergara M E, Ortiz Rebollo A, Alvarez J R and Rivera M 2008 *J. Phys. Chem. Solids* **69** 1

Schmeisser D, Rager A, Thonke K, Pilkuhn M, Frohlich D, Gaauglits G, Schafer M and Oelkrug D 1991 *Synth. Met*. **41** 1457

Seoudi R, El-Bahy G S and El Sayed Z A 2006 *Opt. Mater*. **29** 304

Shafai T S and Anthopoulos T D 2001 *Thin Solid Films* **398** 361

Tauc J 1972 *'Optical properties of non-crystalline solids'*, in *Optical properties of solids*, F Abele's (ed.), (Amsterdam: North-Holland Publishing Co.) p. 277

Wojdyla M, Bala W, Derkowska B, Rebarz M and Korcala A 2008 *Opt. Mater*. **30** 734